ACS APPLIED MATERIALS & INTERFACES

Research Article

www.acsami.org

Highly Populated and Nearly Monodispersed Nanosilica Particles in an Organic Medium and Their Epoxy Nanocomposites

Wenqi Yu,[†,‡] Jifang Fu,*[,†] Xing Dong,[†] Liya Chen,[†] Haisen Jia,[†] and Liyi Shi[†,‡]

[†]Nano-Science & Technology Research Center and [‡]Department of Chemistry, College of Science, Shanghai University, 99 Shangda Road, Shanghai 200444, People's Republic of China

ABSTRACT: An organic aminopropyl-functionalized nanosilica sol was synthesized in the presence of ethyl silicate, γ-(aminopropyl)-triethoxysilane (KH550), and *N*,*N*-dimethylformamide (DMF) via a sol–gel technique and then used to prepare epoxy nanocomposites. Structure and morphology analyses of the obtained aminopropyl-functionalized nanosilicas were observed by dynamic light scattering (DLS), transmission electron microscopy (TEM), and high-resolution TEM (HRTEM). TEM and DLS showed that modified nanosilicas with an average diameter of 30 nm dispersed homogeneously in DMF. The effects of the aminopropyl-functionalized nanosilica particles on the flexural modulus, impact strength, glass transition temperature (T_g), and bulk resistivity (ρ_v) of the epoxy nanocomposites were investigated. The toughening mechanisms and microstructures were determined in terms of the impact fracture surface morphology using scanning electron microscopy.

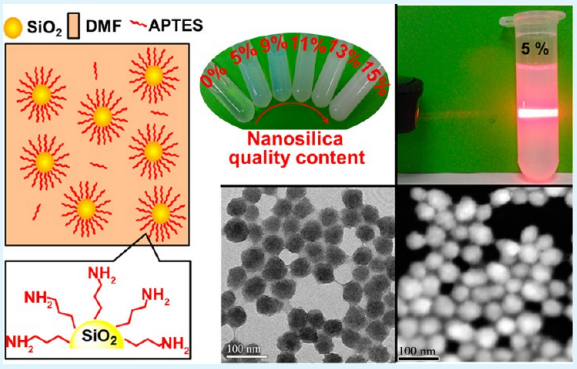

KEYWORDS: *sol–gel, nanosilica sol, epoxy, nanocomposites, bulk resistivity*

1. INTRODUCTION

Nanoparticles are widely used in nanotechnology, biological medicine, and materials science.[1,2] The incorporation of nanoparticles into various polymers is beneficial to improving the physical properties, thermal stability, and mechanical strength.[3,4] Epoxy resins (EPs) are extensively used as adhesives, coatings, matrixes of composites, casting applications, and electronic encapsulating compounds. However, the commonly used EPs are brittle because of their inherently high cross-linking structures. Therefore, several methods have been adopted to overcome their brittleness. EP filled with nanoparticles to overcome their brittleness and to prepare high-performance nanocomposites are getting more and more researchers' attention.[4−11] Nanoparticles have some unique properties such as high specific surface area compared to microparticles, which can promote the transfer of external stress from polymer matrixes to nanoparticles and improve the modulus and strengths of the polymers to a higher level than microfillers. Moreover, the necessary loading content of nanoparticles in a polymer matrix is normally much lower compared to microfillers, and nanocomposites exhibit significantly improved properties.[12−14]

Nanosilica particles are interesting for their applications in the field of electronic components and nanomedicine.[1,15−17] Silica is the most widely used filler to modify epoxy to improve the thermal stability and decrease the internal stress. However, nanosilica particles are more susceptible to aggregation than microparticles because of the increment in the surface silanol structure and high surface energy. The reduced number of hydrogen-bonded water molecules on the nanosilica particle surface and a weaker reactivity to the silane coupling agents result from an increase in the amount of isolated silanol groups.[18] Nanoparticles disperse with difficulty in the polymer matrix, which limits their application. This trend is especially obvious with the high content of nanoparticles.

Recently, nanosilica particle sols in an aqueous or ethanol medium were mainly used to prepare silica–epoxy nanocomposites instead of a direct-filling dispersion of nanoparticles. However, the solubility of neat epoxy in the aqueous or ethanol medium is very poor, and some small-molecule residuals may be in the nanosilica sol, which leads to an irreversible decrease in the insulation resistance and dielectric performance of the EP nanocomposites. The properties and behavior of nanocomposites strongly depend on the nanoparticle compatibility and dispersion between the nanoparticles and polymer matrix. To meet the fast development of the electronic information industry, better performances of adhesives, substrates, and electronic packaging materials are required such as low viscosity, low dielectric loss, high mechanical properties, high electric insulation, and high thermal properties. Therefore, the development of high uniformly dispersed and high-performance silica–epoxy nanocomposites has become an inevitable trend and a large challenge.

Therefore, using nanosilica sol in an organic medium to prepare nanocomposites is a novel application field for nanosilica

Received: April 3, 2013
Accepted: August 28, 2013
Published: August 28, 2013

particles that brings forth very strict requirements of dispersity, stability, and high purity. Our designed objective was to achieve aminopropyl-functionalized nanosilica particles in organic media with a low water content that can be used in the field of electronic components and can evidently improve the physical and dispersion properties of nanosilica particles in the polymer matrix. In this research, we describe a new way to synthesize a novel organic nanosilica sol in an organic solvent and then use it to prepare silica−epoxy nanocomposites with different nanosilica contents through a special sol−gel process. The aminopropyl-functionalized nanosilica particles can disperse homogeneously in an organic solvent (DMF) or epoxy matrix, and the solubility of neat epoxy in the organic solvent is better than that in water and ethanol. So far, this is a new and simple approach to preparing high-content, stable, monodispersed nanosilica particles in an organic medium. The organic nanosilica sol was characterized in detail. The impact strength, flexural modulus, thermal resistance, thermal stability, and electrical insulating properties of the epoxy nanocomposites were investigated and discussed.

2. EXPERIMENTAL SECTION

2.1. Chemical Materials. Ethyl silicate, *N*,*N*-dimethylformamide (DMF), ammonia solution, and triethanolamine (Sinopharm Chemical Reagent Co., Ltd., China, analytical grade), γ-(aminopropyl)-triethoxysilane (APTES; Shanghai Yaohua Chemical Co., China), and epoxy resin (EP, and diglycidyl ether of bisphenol A, epoxy equivalent weight = 185−210 g equiv^{-1}) (provided by Yueyang Chemical Co., China) were used. The curing agent was methylhexahydrophthalic anhydride (MeHHPA; Yangzhou Guangrun Chemical Co., Ltd., China) and was used without further purification. Triethanolamine was used as the curing accelerator.

2.2. Preparation of Nanosilica−DMF Sols. An appropriate amount of an ammonia solution and APTES were dissolved in a certain amount of DMF in a 250 mL three-necked flask. Ammonia solutions were used as catalysts for hydrolysis. The solution was composed of ethyl silicate and DMF in a molar ratio of 1:5 and next slowly dropped into the 250 mL three-necked flask at ambient temperature with stirring for 48 h. After that, the mixture was aged for 7−15 days. DMF−nanosilica sols with different solid contents (5, 9, 11, 13, 15 wt % relative to DMF) were prepared. DMF−nanosilica sol was kept at 4 °C until use. Figure 1 shows detailed structures and real pictures of nanosilica−DMF sols.

2.3. Preparation of Nanosilica−EP Sols. EP was added to the obtained nanosilica−DMF sol with mechanical stirring for 10−12 h. Then DMF was completely removed from the mixture by distillation in a vacuum at 70 °C. The sol of nanosilica−EP (nanosilica solid content, 0−30 wt % relative to the epoxy) was kept at 4 °C until use, and the results are given in Figure 2a.

2.4. Curing Procedure. A stoichiometric amount of curing agent and an appropriate amount of curing accelerator were added into the nanosilica−EP sol and then mechanically stirred for 30 min. The obtained mixtures were repeatedly degassed in a vacuum at 80 °C for approximately 10 min until there were no trapped bubbles. Finally, the mixture was poured into an aluminum mold. The curing procedure was carried out: 1 h at 100 °C + 5 h at 120 °C + 10 h at 150 °C + 2 h at 160 °C. A series real pictures of nanocomposites with different nanosilica contents (nanosilica content, 0−20 wt % relative to the epoxy nanocomposites) and the possible interactions occurring in the nanocomposite are displayed in Figure 2b−d. Details of the key properties obtained in this investigation are listed in Table 1.

2.5. Materials Characterization. The morphology and dispersion quality of the nanoparticles were investigated by a JEOL 200CX transmission electron microscope at an acceleration voltage of 200 kV. High-resolution transmission electron microscopy (HRTEM) was applied to observe the core−shell structure of the nanosilica−DMF sols using a transmission electron microscope equipped with an energy-dispersive X-ray (EDX) spectrometer.

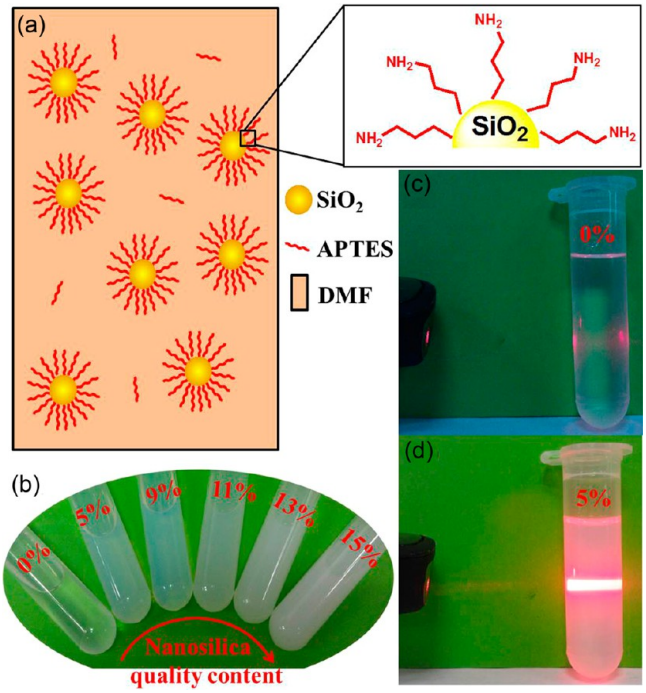

Figure 1. (a) Schematic diagram of the nanosilica homogeneously dispersed mechanism. (b) Organic nanosilica sols. (c and d) Observed light scattering due to the presence of nanosilica particles in the nanosilica−DMF sols upon showing a red laser beam through the samples.

The particle sizes of nanosilica particles was determined through dynamic light scattering measurement with a Zetasizer 3000HS.

Fourier transform infrared (FTIR) spectroscopy of the nanosilica−EP nanocomposites were performed on a Nicolet Avatar370 FTIR instrument (Thermo Nicolet, USA) in the range from 400 to 4000 cm^{-1} using KBr pellets.

According to China National Standard GB1843-1996, an impact tester was used to determine the no-notch impact strengths of the nanocomposites. The flexural modulus was measured on an Instron electron omnipotence tester according to ASTM D790-2010. The average value for each nanocomposite was recorded at least three times through repeated measurements.

The fracture surfaces after the impact strength test were sputtered with gold and examined using scanning electron microscopy (SEM; JSM-6700F, Japan) at an accelerating voltage of 15.0 kV.

The possible unreacted hardener fraction was tested by selective extraction according to China National Standard GB/T 2576-2005. These samples were processed into powder and placed in acetone for 12 h at approximately 80 °C to extract the residual uncured component. The process was conducted three times, and then the powders were placed in a vacuum-drying oven at 110 °C (−0.1 MPa), drying to constant weight.

Dynamic mechanical thermal analysis (DMTA) of samples with the dimension 35 × 10 × 2 mm^3 was carried out on a dynamic mechanical analyzer (DMA Q800, TA Instruments Inc., USA) from room temperature to 260 °C at a heating rate of 5 °C min^{-1}. The frequency used was 1.00 Hz.

The volume resistivity (ρ_v) and surface resistivity (ρ_s) of the samples were measured using a high resistance meter (4339B; Agilent, USA) and a resistivity cell (16008B; Agilent, USA) according to ASTM D257-2007. At least three scans of every sample were taken in order to get better accuracy. The surface (1) and volume (2) resistivity can be calculated by the following equations:

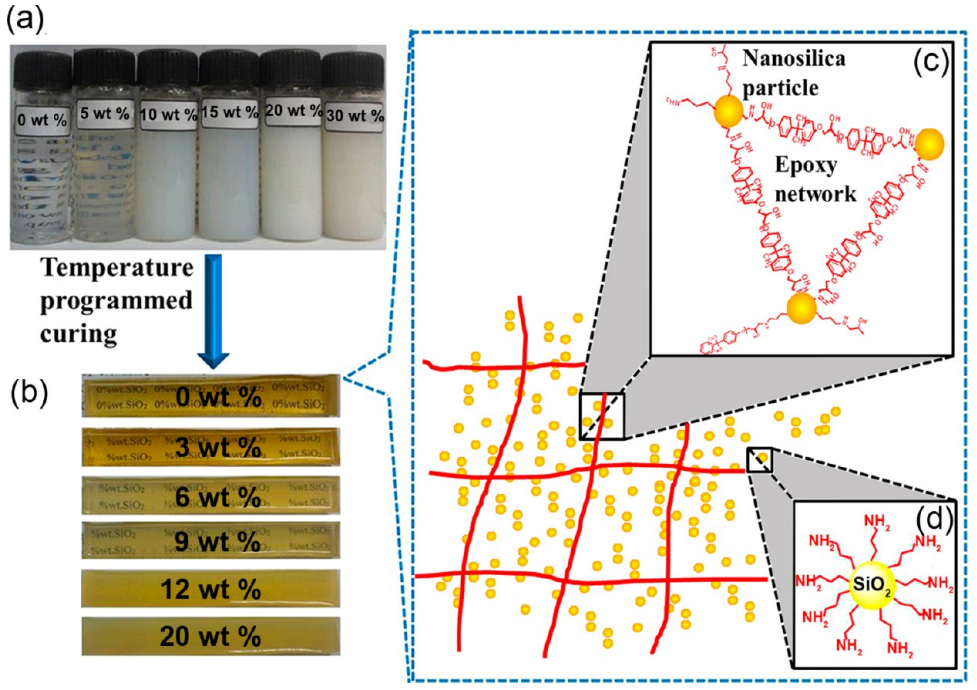

Figure 2. (a and b) Representation of the route from nanosilica–EP sols to nanosilica–EP nanocomposites. (c) Epoxy chain–nanosilica–epoxy chain. (d) Core–shell structures formed by interaction of APTES with the nanosilica.

Table 1. Compositions of the Nanosilica Sol and Key Properties of the Nanosilica–EP Nanocomposites with Different Nanosilica Contents

	nanosilica content (wt %)		nanosilica content in nanocomposites							
sample code	DMF sols	EP sols	vol % (φ_p)	wt %	curing degree (%)	T_g(DMTA) (°C)	impact strength (kJ m^{-2})	flexural modulus (MPa)	surface resistivity ($\times10^{17}\Omega$)	bulk resistivity ($\times10^{14}\Omega$·m)
S_0	0	0	0	0	92.73	121.6	15.50	3138.38	0.24	0.71
S_1	5	5	1.60	3	98.19	93.9	17.53	3293.24	0.015	0.63
S_2	9	10	3.17	6	99.83	110.8	29.55	3255.39	0.15	1.25
S_3	11	15	5.33	9	97.08	105.2	40.11	3355.24	0.689	2.24
S_4	13	20	7.33	12	96.65	113.5	31.62	3338.09	2.67	1.56
S_5	15	30	11.93	20	95.43	89.0	22.20	3888.09	13.5	1.44

$$\rho_s = \frac{\pi(D_1 + D_2)}{D_2 - D_1} R_s \quad (1)$$

$$\rho_v = \frac{\pi\left(D_1 + \frac{B(D_1 - D_2)}{2}\right)^2}{4t} \frac{R_v}{10} \quad (2)$$

where D_1 and D_2 are the diameters of the main (mm) and ring (mm) electrodes, respectively, B is the effective area coefficient (1 for ASTM D257-2007), t is the thickness of test material (mm), R_s is the surface resistance, and R_v is the volume resistance.

A NETZSCH thermal gravimetric analyzer (TG 209 F3) was used to observe the thermal degradation behavior of the nanosilica–EP nanocomposite (approximately10 mg) in a nitrogen atmosphere from 25 to 700 °C at a heating rate of 10 °C min^{-1} in all cases. The initial thermal decomposition temperature (T_{IDT}, °C) was 10 wt % of weight loss of each sample.

3. RESULTS AND DISCUSSION

3.1. Morphology of Nanosilica–DMF and Nanosilica–EP Sols. Figure 1a gives the schematic diagram of the aminopropyl-functionalized nanosilica homogeneous dispersion mechanism. The silica nanoparticles are coated with APTES, which improves the nanoparticle dispersion. As shown in Figure 1b, organic nanoparticle sols are homogeneous and become more opaque with increasing solid content. As displayed in Figure 1c,d, the organic nanosilica sols show the Dindar phenomenon. A red laser beam was shone through the solutions, and the observed light scattering emerges because of the presence of nanosilica particles in the nanosilica–DMF sols.

TEM micrographs of the nanosilica–DMF sols with 9, 13, and 15 wt % nanosilica particle content are shown in Figure 3. These images show well-dispersed silica nanoparticles in DMF. The average diameter size of nanosilicas at 9 wt % is about 30 nm, as shown in Figure 3d. No obvious particle agglomerations are observed. In Figure 3e,f, aggregation phenomena were avoided because the nanosilica particles are surface-functionalized by APTES (just like organic coatings), which will improve the compatibility of the nanosilica particles in the organic medium. Through the high-angle annular dark-field (HAADF) mode of HRTEM, the high-brightness white dots are nanosilica particles, which were coated with APTES and constituted a core–shell structure. Note that surface modification plays an important role for monodisperse nanosilica particles.

dx.doi.org/10.1021/am402845d | ACS Appl. Mater. Interfaces 2013, 5, 8897–8906

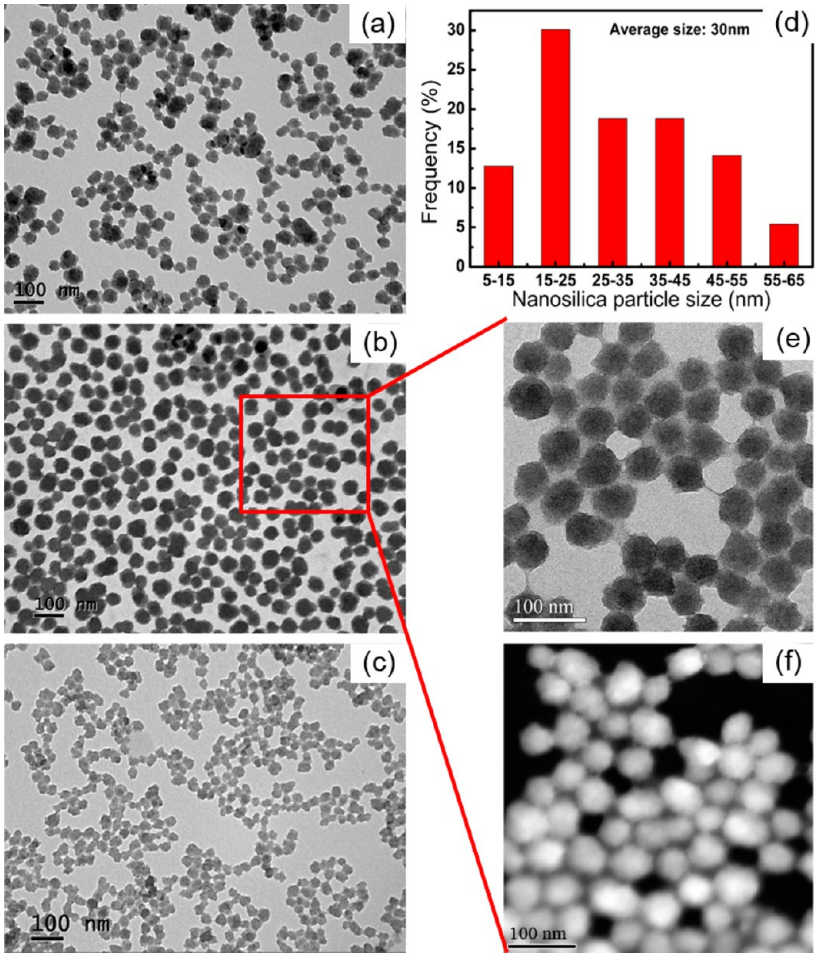

Figure 3. TEM micrographs of the nanosilica–DMF sols: (a) 9 wt %; (b) 13 wt %; (c) 15 wt %. (d) Particle size distribution of the nanosilica–DMF sol at 9 wt % content. (e) HRTEM image of the 13 wt % nanosilica–DMF sol. (f) HAADF mode.

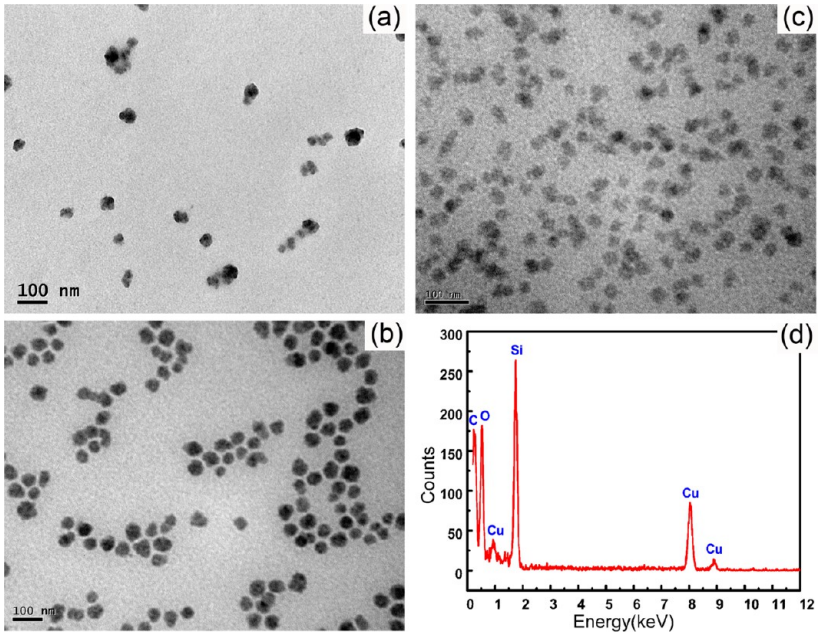

Figure 4. TEM micrographs of the nanosilica–EP sols: (a)10 wt %; (b) 20 wt %; (c) 30 wt %. (d) EDX spectrum of the 20 wt % nanosilica–EP sol.

TEM micrographs of the nanosilica–EP sols containing 10, 20, and 30 wt % nanosilica particles are given in Figure 4. The dark dot parts are the nanosilica particles and the gray part is the EP matrix, which is confirmed by using EDX measurement in Figure 4d. The particle number increased with an increase in the nanosilica content. Uniformly dispersed nanosilica particles

dx.doi.org/10.1021/am402845d | ACS Appl. Mater. Interfaces 2013, 5, 8897–8906

without aggregation phenomena are observed in the EP matrix. This is attributed to the aminopropyl functionalization, which changes the surface of the nanosilica particles from hydrophilicity to hydrophobicity and can give a better compatibility between the nanosilica particles and EP matrix.[19]

3.2. Formation of the Nanosilica−EP Nanocomposites. As shown in Figure 2, the nanosilica−EP nanocomposites are transparent up to 9 wt %, and this suggested that no macroscopic phase separations emerged at least on the scale of visible light. Besides the curing reaction between MeHHPA and EP, the cross-linking reaction between EP and aminopropyl-functionalized nanosilica particles could additionally be involved in the case. The possible structure and networks are given in Figure 2c,d.

FTIR spectra of pure EP and nanosilica−EP nanocomposites are shown in Figure 5, indicating which bonds formed or

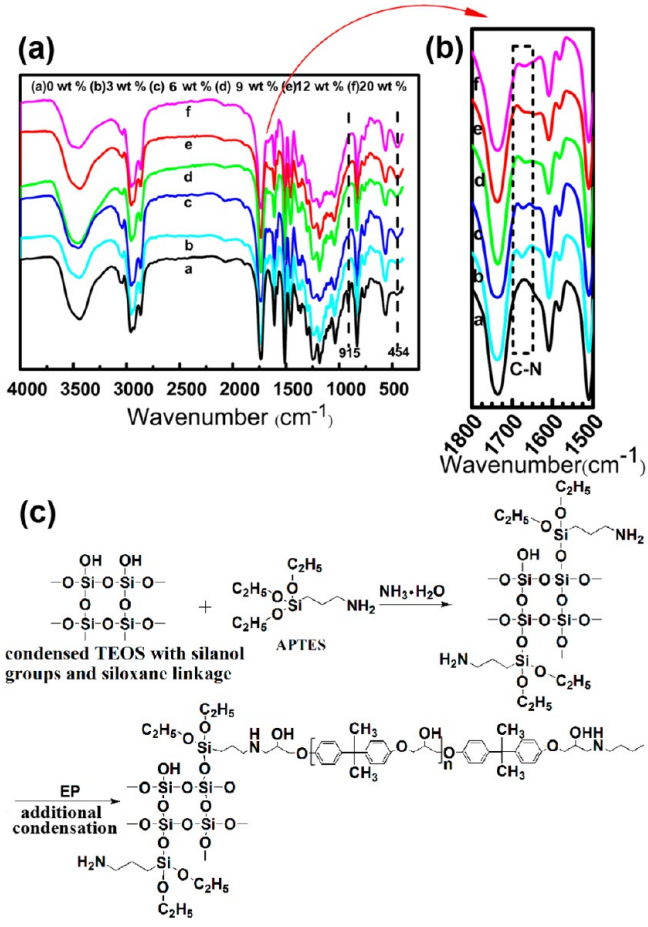

Figure 5. (a) FTIR spectra of nanosilica−EP hybrid materials with different contents of nanosilica: 0 (pure EP), 3, 6, 9, 12, and 20 wt %. (b) Enlarged formation displaying the C−N peak that emerged because of chemical interaction between the amino and epoxy groups. (c) Schematic representation of the possible reaction mechanism.

disappeared during the special sol−gel and curing procedure and elucidating whether nanosilica−EP nanocomposites are a covalently bound network or simply a physical mixture. The characteristic peak at 483 cm^{-1} and the broad-band absorption of nanosilica−EP nanocomposites appearing at 1000−1100 cm^{-1} correspond to the bending vibrations and asymmetrical stretching[20,21] in Si−O−Si bonds, respectively. The asymmetrical stretching and bending vibrations are more and more obvious with the addition of nanosilica particles. The stretching vibration absorption peak of the epoxy group emerged at 915 cm^{-1}; the epoxy group peak became weak and even disappeared with an increase in the nanosilica content, which indicates that the Si−O−Si network structure promotes the curing process of the EP system. Upon comparison of the FTIR spectra of neat epoxy and nanosilica−EP nanocomposites in Figure 5b, we find that all of the nanosilica−EP nanocomposites show a characteristic peak at around 1680 cm^{-1}, which elucidates that new C−N bonds are formed in the nanosilica−EP nanocomposites through cross-linking between APTES on the surface of nanosilica and EP. The possible reaction mechanism is shown in Figure 5c.

3.3. Mechanical Properties. It is known that the weak bonding between the fillers and polymer matrix will result in a decline in the flexural modulus of a microparticle-filled composite with increasing filler content.[22,23] The flexural modulus of the microparticulate composite can be improved compared to that of the polymer matrix when the bonding between the fillers and polymer matrix is strong enough.[24] Figure 6a gives flexural modulus results of nanosilica−EP nanocomposites. It can be observed that the flexural modulus increases with increasing nanosilica content, indicating that strong bonding between the nanosilica particles and epoxy networks occurs and the nanosilica−EP networks can withstand external stress. From the curve, at 20 wt % nanosilica content, the flexural modulus of nanosilica−EP nanocomposites is 3888.1 MPa, and this is 24% higher compared to pure EP.

The impact strength of the nanosilica−EP nanocomposites containing different nanosilica contents is displayed in Figure 6b. The impact strength is remarkably improved with an in crease in the nanosilica content, and the highest value is 40.11 kJ m^{-2} at 9 wt % nanosilica content, which is 159% higher than that (15.50 kJ m^{-2}) of pure EP. The main reason is that uniformly nanosilica particles have a large amount of surface-active centers, and they can tightly combine with the epoxy matrix by a grafting reaction. When subjected to an external force, the nanoparticles do not easily break away from the epoxy matrix and transfer the external force very well. Then the local yield deformation occurs in the surrounding matrix and dissipation of the impact energy increases,[25] resulting in a toughening of the nanosilica−EP nanocomposites. However, when the nanosilica content is excessive, nanoparticle aggregation and the microcracks of the nanocomposites are very big and almost develop into a stress cracking, leading to a decrease in the impact strength.

In recent years, the correlations between the improvements in the mechanical properties of the nanocomposites and the interparticle distance attracted the wide attention of researchers. Wu[26] proposed the critical interparticle distance model in order to interpret the toughening and strengthening mechanisms in the rubber-modified brittle polymer materials. This model in view of the hypotheses of ideal dispersion and cubic structure and the model function used was the following:

$$\frac{\tau}{d} = \left(\frac{\pi}{6\varphi_p}\right)^{1/3} - 1 \qquad (3)$$

where τ is the interparticle distance, d is the particle diameter, and φ_p is the volume filler content. The volume filler content (φ_p) is calculated according to the following equation, and the results are listed in Table 1:

dx.doi.org/10.1021/am402845d | ACS Appl. Mater. Interfaces 2013, 5, 8897−8906

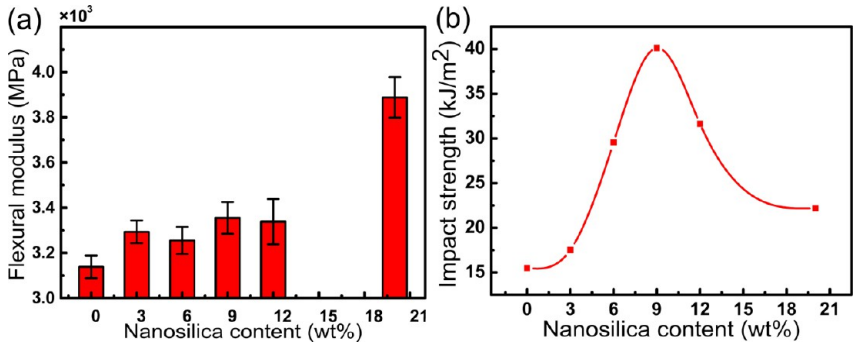

Figure 6. (a) Flexural modulus and (b) impact strength of nanosilica–EP nanocompositesite.

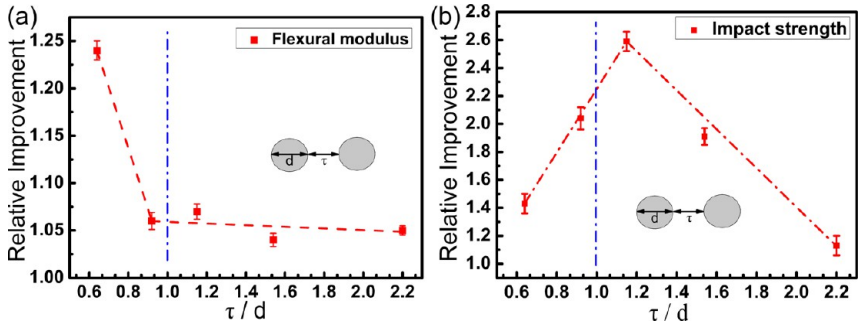

Figure 7. Correlations between the interparticle distance and mechanical properties.

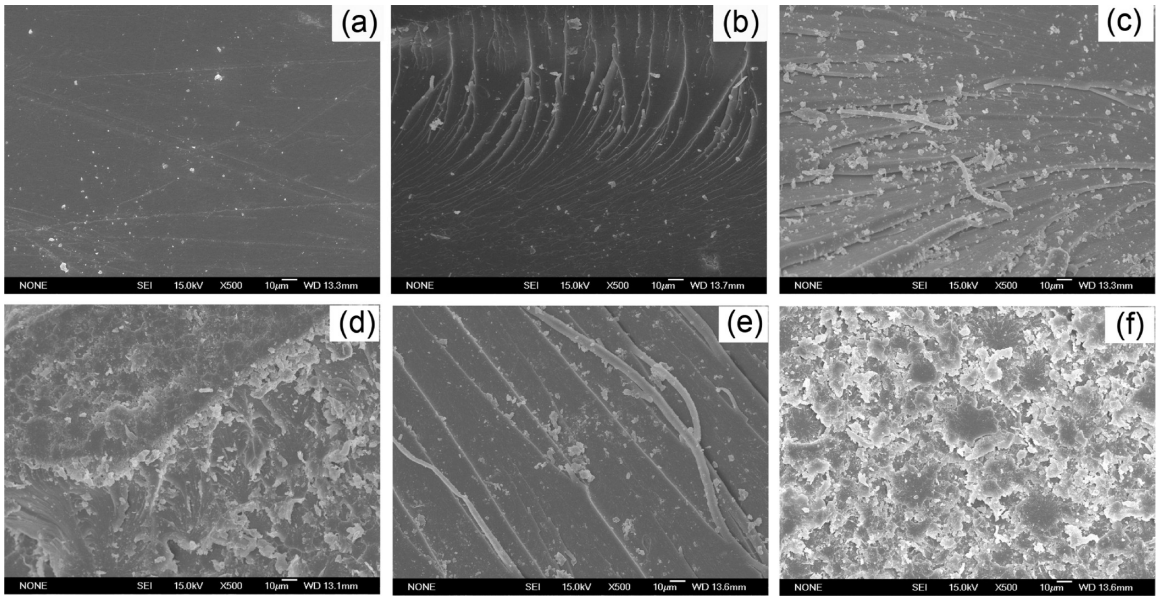

Figure 8. Low-magnification SEM micrographs of nanosilica–EP nanocomposites from impact tests with different nanosilica contents: (a) neat epoxy; (b) 3 wt %; (c) 6 wt %; (d) 9 wt %; (e) 12 wt %; (f) 20 wt %.

$$\varphi_p = \frac{W_f}{W_f + (1 - W_f)\frac{\rho_f}{\rho_m}} \quad (4)$$

where W_f is the filler content by weight and ρ_f and ρ_m are the densities of the filler and polymer matrix, respectively. Young's modulus and the impact strength of the nanosilica–EP nanocomposites versus τ/d are shown in Figure 7. It can be discovered that Young's modulus improves more remarkably with a further decrease of the ratio (τ/d) and the impact strength increases with a reduction of the ratio over 1.2. It is assumed that this phenomenon is because the nanosilica particles are close enough to fabricate a three-dimensional EP network around them, as discussed by others.[27] However, as shown in Figure 7b, it can be found that improvement of the impact strength becomes very small when the nanosilica particle content is up to 12 wt % and the ratio of τ/d is below 1.0. Therefore, the new toughening mechanism that particle flocculation at high content reduces the toughening efficiency of polymer blends proposed by Qi et al.[28] should be taken into account.

3.4. Morphology of Fractographs. SEM of the impact fracture surface partly shows some fracture mechanisms of the nanosilica–EP nanocomposites. With the addition of silica

dx.doi.org/10.1021/am402845d | ACS Appl. Mater. Interfaces 2013, 5, 8897–8906

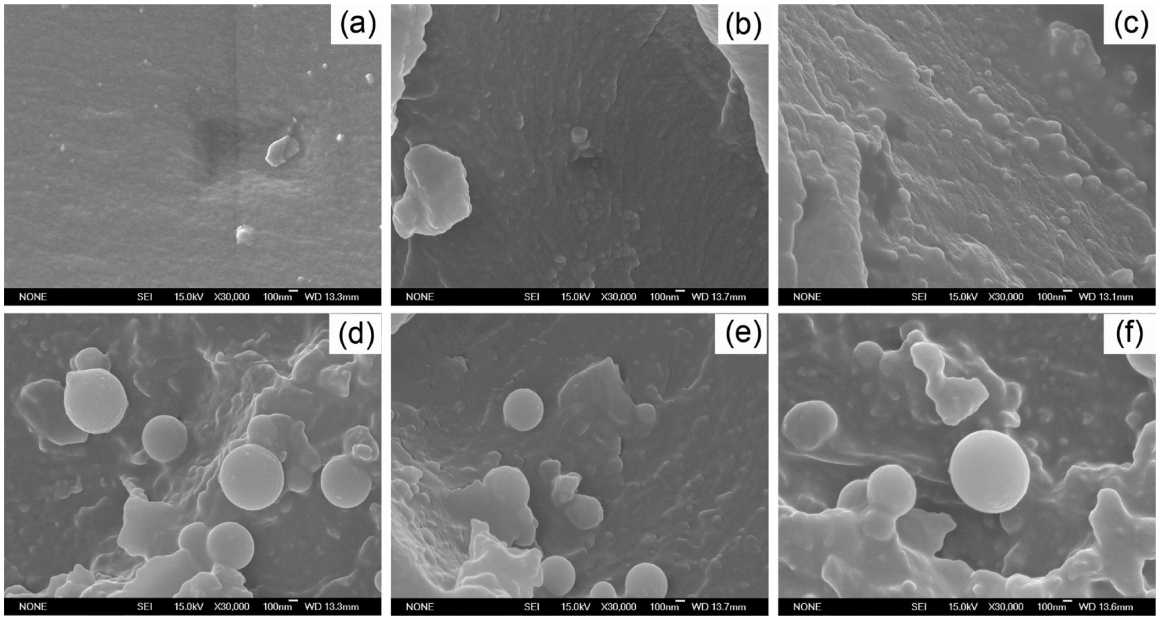

Figure 9. Higher magnified SEM images of the neat EP and nanosilica–EP nanocomposites from impact tests with different contents of nanosilica: (a) neat epoxy; (b) 3 wt %; (c) 6 wt %; (d) 9 wt %; (e) 12 wt %; (f) 20 wt %.

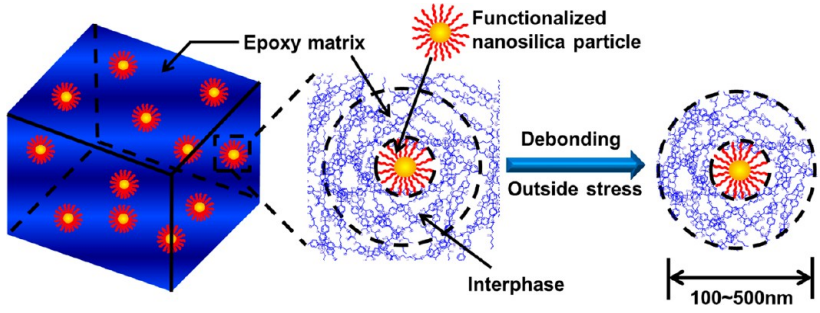

Figure 10. Schematic drawing showing the core–shell structure of a functionalized nanosilica particle coated with EP layers.

nanoparticles, a much rougher and irregular fracture surface emerges, as seen in Figure 8b–f.

Many dimples, numerous crazings with river shape, and drawing filar phenomena appear in the impact fracture surface of the nanosilica–EP nanocomposites, which may be attributed to the blocking effects and crack pinning of nanosilica particles in the epoxy network matrix.[29,30] In addition, many of river-shaped lines are sinuous, which means the crack fronts are often deflected and stopped because of interactions between the particles and crack, which are probably beneficial to the fracture toughness by releasing the external stress around the crack fronts.[27] Kinloch et al.[3] also observed a similar trend, in whose work a possible toughening mechanism is crack bowing. The formation of these phenomena is due to rigid nanosilica fillers, which induced the matrix around the nanosilica producing significant plastic deformation under tension, indicating that much fracture energy is likely dissipated. In contrast, as illustrated in Figure 8a, the unfilled epoxy exhibits a large smooth area with clear fracture boundaries, which means the crack propagation resistance is small and there is almost no plastic deformation, indicating a typical brittle fracture.

This can be clearly observed in high-magnification SEM images in Figure 9. The neat epoxy surface is flat; however, spherical nanosilica particles can clearly be observed in the nanosilica–EP nanocomposites. In addition, the spheres can homogeneously disperse in the epoxy matrix with no obvious agglomerations, which agree with the TEM images of nanosilica in Figures 3 and 4. As shown in Figure 9, the diameter of the spherical particles is in the scope of approximately 100–200 nm (some particles are even larger), and this is obviously greater than the diameter of monodispersed nanosilica particles in TEM in Figure 4. This is due to the fact that the nanosilica particles were surface-functionalized by a silane coupling agent, which can react with both the EP matrix and inorganic particles and bring about strong chemical interactions between them. Figure 10 is a simulated diagram about the existing form of nanosilica particles in the EP matrix; the aminopropyl-functionalized nanosilica particles were coated with EP layers just like a core–shell structure. Furthermore, the debonding process may occur somewhere within the matrix under huge external stress, resulting in the unique morphology of impact fractured surfaces, as seen in Figure 9d–f, and finally leading to an energy-dissipating toughening mechanism. With an increase in the nanosilica particle content, the interparticle distance decreases, this debonding phenomenon increases, and more impact energy is absorbed, which finally significantly improves the performance of the nanosilica–EP nanocomposites at around 9–12 wt % nanosilica content. These core–shell structures can greatly influence the fracture behavior at a critical interparticle distance, which corresponds to the particle content. Moreover, when the

dx.doi.org/10.1021/am402845d | ACS Appl. Mater. Interfaces 2013, 5, 8897–8906

nanosilica particle content is further increased, particle aggregation increases, the phase microstructure changes, and the matrix ligament increases,[28] which finally leads to a decline in the performance of the nanosilica−EP nanocomposites. On the basis of the analysis above, the toughness is determined by the particle content, particle dispersion, and changes of the matrix and phase morphology.

3.5. Surface Resistivity and Bulk Resistivity. The surface resistivity (ρ_s) and bulk resistivity (ρ_v) are used to estimate the electrical insulating properties of the nanosilica−EP nanocomposites, and the detailed results are listed in Table 1 and Figure 11. The surface resistivity and bulk resistivity show

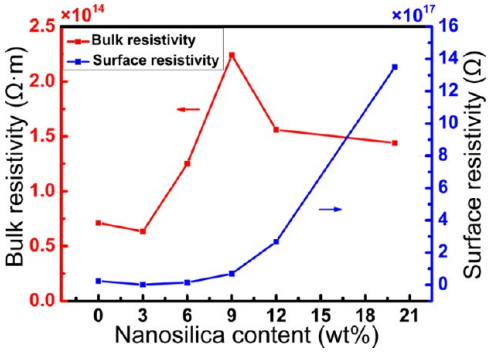

Figure 11. Bulk resistivity and surface resistivity of the nanosilica−EP nanocomposites.

increasing trends with the addition of fillers. The surface resistivity increases with increasing filler content. The bulk resistivity increases sharply over the 3 wt % nanosilica content and attains an optimal value at 9 wt %. This is can be explained by the facts that the higher content nanosilicas result in a tighter three-dimensional network structure and homogeneous nanosilica particles limit migration of the conductive ion. At the same time, nanosilica particles having high surface energy and a large specific surface area can easily adsorb more impurities such as water. Further, the impurities can generate the conductive ion, resulting in a decline in ρ_v. With an increase in the nanosilica particle content over the optimal value, aggregation occurs and the effective nanosilica particles serving as cross-linking points decrease, and these aggregated nanoparticles act as impurities, resulting in a decline in ρ_v. From the analysis above, it can be concluded that the nanosilica particles can substantially improve the electrical insulating properties of the epoxy matrix, although there is a slight decline in ρ_v when the nanosilica content is higher than 9 wt %.

3.6. DMTA. Figure 12a shows the DMTA curves of the nanosilica−EP nanocomposites. The storage modulus improves dramatically with an increase in the nanosilica content at lower temperatures. This is probably because the network structure of Si−O−Si limits movement of the EP molecular chain. With a rise in temperature, the nanosilica−EP nanocomposites go into the rubbery state very early, resulting in a slightly lower storage modulus compared to that of pure EP. So, the plasticizing effect of colloidal nanosilica cannot be ignored.

Figure 12b shows the T_g values of nanosilica−EP nanocomposites derived from the peak position corresponding temperature of the loss factor curves. T_g of the nanocomposites decreases in comparison with pure EP; this similar phenomenon is also observed by other researchers.[27,31] Some researchers have proposed a plasticizing effect of functionalized nanosilicas to explain this phenomenon according to studies by Zhang et al.,[27] Huang and Lee,[32] and Tarrío-Saavedra et al.[33] The plasticizing effect of functionalized nanosilicas may result from the effect of absorbed moisture or residual small organic molecules[34] or the small gap between the nanosilica interface and resin.[35] In order to investigate whether there is uncured EP and its effects on the glass transition temperature, the possible fraction of unreacted hardener or EP was measured by selective extraction tests. The curing degrees of samples were listed in Table 1. From Table 1, we find that the nanocomposites show higher curing degrees than pure EP and the values are higher than 95%, so we can say that the nanosilica−EP nanocomposites have been cured completely. That means that shifting of the glass transition temperature to lower temperatures cannot be attributed to uncured EP. T_g values of the nanosilica−EP nanocomposites increase with an increase in the content of the nanosilica particles up to 12 wt %; this was attributed to the facts that the incorporation of uniformly dispersed nanosilica restricts polymer chain movement and increasing effective cross-linking densities result from the amine group of nanosilica reacting with epoxy at certain contents. When the filler content was further increased to 20 wt %, the T_g values of the nanocomposites decrease, indicating some discontinuity of the polymer matrix and macroscopic phase separations, which would not be sufficient to surround all of the particles and agglomerates.[33] This is also attributed to particle aggregation, which decreases the effective nanoparticles as physical cross-linking sites and cross-linking densities and thus finally decreases the T_g values of the nanocomposites.

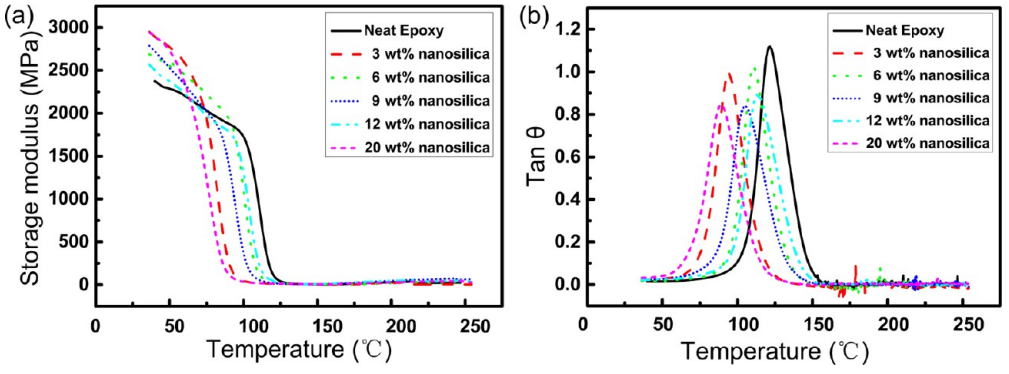

Figure 12. DMA results for nanosilica−EP nanocomposites with various contents of nanosilica: (a) storage modulus curves; (b) loss factor (tan θ) curves.

dx.doi.org/10.1021/am402845d | ACS Appl. Mater. Interfaces 2013, 5, 8897−8906

3.7. Thermogravimetric Analysis (TGA). TGA can not only give important structural information but also investigates the stability of materials. Figure 13 gives the TGA thermogram

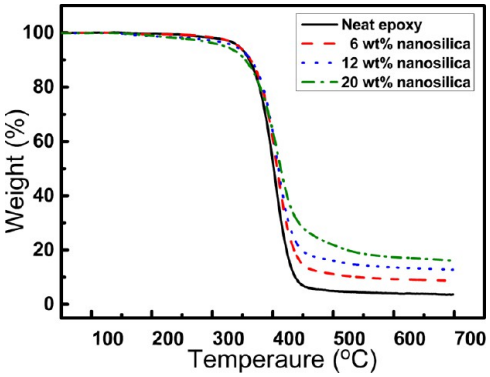

Figure 13. TGA curves of pure EP and nanosilica–EP nanocomposites in a nitrogen atmosphere.

curve for pure EP and nanosilica–EP nanocomposites. The initial thermal decomposition temperatures [T_{IDT} (°C)], the temperatures of the maximum decomposition rate [T_{max} (°C)], and the final char yields at 700 °C are also summarized in Table 2.

Table 2. Thermal Stability Properties of Nanosilica–EP Nanocomposites Calculated from TGA Curves

sample code	theoretical content (wt %)	T_{IDT} (°C)	T_{max} (°C)	char yield (%) at 700 °C
S_0	0	360.7	402	3.6
S_2	6	363.3	406	8.7
S_4	12	364.5	408	12.8
S_5	20	354.3	410	16.1

As shown in Figure 13 and Table 2, it is obviously seen that each TGA curve has only one degradation stage. At 12 wt % nanosilica content, the T_{IDT} value (364.5 °C) of the nanosilica–EP nanocomposite is higher than that (360.7 °C) of pure EP. In addition, nanosilica–EP nanocomposites have higher maximum decomposition temperatures than those of pure EP, and these T_{max} values increase with increasing nanosilica content. The T_{max} value at 20 wt % nanosilica content is 8 °C higher than that of pure EP. It can be observed that, from the results of TGA, the thermal stability of these nanosilica–EP nanocomposites is slightly improved. The behavior is attributed to the existence of cross-linking Si–O–Si in the nanosilica–EP nanocomposites and the strong chemical interaction between the EP matrix and functionalized nanosilica particles, which inhibit the molecular mobility of polymer chains.[36] In addition, TGA can be used to provide the actual inorganic particle content in the organic–inorganic materials.[37] Because most of the organic polymer had decomposed before 700 °C in a nitrogen atmosphere (however, inorganic moieties can usually withstand 1000 °C), the char yield should be the actual content of the inorganic part.[38,39] Table 2 shows the char yield of the nanosilica–EP nanocomposites over 700 °C; the results approximately correspond to the theoretical inorganic nanosilica particle loadings.

4. CONCLUSIONS

The organic nanosilica and EP nanosilica sols with homogeneously dispersed nanosilica particles are successfully synthesized by a special sol–gel technique and then used to prepare epoxy nanocomposites. TEM and HRTEM analyses indicate that nanosilica particles can disperse homogeneously in DMF or pure EP. The effects of aminopropyl-functionalized nanosilica particles were remarkable. The impact strength, flexural modulus, bulk resistivity, and surface resistivity of the nanosilica–EP nanocomposites improve with nanosilica particle addition, and this method can achieve highly populated nanosilica particles in an organic medium. The addition of nanosilica increases the impact strength and flexural modulus of nanosilica–EP nanocomposites about 2.59 and 1.24 times at 9 and 20 wt % nanosilica particle content, respectively. SEM observation of the fracture surface showed numerous crazings with river shape, drawing filar phenomena, and a lot of dimples and nanosilica particle coating with the epoxy matrix, which were obviously credited for increases in the toughness of nanosilica–EP nanocomposites. SEM at high magnification indicates that the silica nanoparticles disperse homogeneously in the epoxy matrix. TGA indicates that nanosilica–EP nanocomposites exhibit improvement in T_{IDT}, T_{max}, and char yield at 700 °C compared to the neat epoxy. The nanosilica–EP nanocomposites at high nanosilica content display significant improvements in the electrical insulation properties and can find applications in the electronic industry, construction industry, etc.

AUTHOR INFORMATION

Corresponding Author

*E-mail: fjfshu@hotmail.com or fjfshu@shu.edu.cn.

Notes

The authors declare no competing financial interest.

ACKNOWLEDGMENTS

We thank the auspices from the Shanghai Leading Academic Discipline Project (Grant S30107), Special Project for Key Project of Chinese Ministry of Education (Grant 208182), Key Subject of Shanghai Municipal Education Commission (Grant J50102), Shanghai University Development Foundation (Grant A.10-0407-11-002), and Program for Professor of Special Appointment (Eastern Scholar) at Shanghai Institutions of Higher Learning (Grant B.39-0411-10-001). The authors acknowledge W. J. Yu, Y. L. Chu, and Instrumental Analysis & Research Center of Shanghai University for assistance with the TEM and SEM observations.

REFERENCES

(1) Nabeshi, H.; Yoshikawa, T.; Matsuyama, K.; Nakazato, Y.; Matsuo, K.; Arimori, A.; Isobe, M.; Tochigi, S.; Kondoh, S.; Hirai, T.; Akase, T.; Yamashita, T.; Yamashita, K.; Yoshida, T.; Nagano, K.; Abe, Y.; Yoshioka, Y.; Kamada, H.; Imazawa, T.; Itoh, N.; Nakagawa, S.; Mayumi, T.; Tsunoda, S. i.; Tsutsumi, Y. *Biomaterials* **2011**, *32*, 2713–2724.

(2) Niemeyer, C. M. *Angew. Chem., Int. Ed.* **2001**, *40*, 4128–4158.

(3) Kinloch, A. J.; Maxwell, D.; Young, R. J. *J. Mater. Sci. Lett.* **1985**, *4*, 1276–1279.

(4) Yee, A. F.; Pearson, R. A. *J. Mater. Sci.* **1986**, *21*, 2462–2474.

(5) Johnsen, B. B.; Kinloch, A. J.; Mohammed, R. D.; Taylor, A. C.; Sprenger, S. *Polymer* **2007**, *48*, 530–541.

(6) Du, J.; Thouless, M. D.; Yee, A. F. *Int. J. Fract.* **1998**, *92*, 271–285.

(7) Fu, J. F.; Shi, L. Y.; Yuan, S.; Zhong, Q. D.; Zhang, D. S.; Chen, Y.; Wu, J. *Polym. Adv. Technol.* **2008**, *19*, 1597–1607.

(8) Schmidt, H.; Jonschker, G.; Goedicke, S.; Mennig, M. *J. Sol–Gel Sci. Technol.* **2000**, *19*, 39–51.

(9) Gomez-Romero, P. *Adv. Mater.* **2001**, *13*, 163–174.

(10) Lan, Q.; Francis, L. F.; Bates, F. S. *J. Polym. Sci., Polym. Phys.* **2007**, *45*, 2284–2299.

(11) Thio, Y. S.; Wu, J.; Bates, F. S. *J. Polym. Sci., Polym. Phys.* **2009**, *47*, 1125−1129.
(12) Wang, K.; Chen, L.; Wu, J. S.; Toh, M. L.; He, C. B.; Yee, A. F. *Macromolecules* **2005**, *38*, 788−800.
(13) Landry, C. J. T.; Coltrain, B. K.; Landry, M. R.; Fitzgerald, J. J.; Long, V. K. *Macromolecules* **1993**, *26*, 3702−3712.
(14) Abramoff, B.; Covino, J. *J. Appl. Polym. Sci.* **1992**, *46*, 1785−1791.
(15) Mallakpour, S.; Dinari, M. *Polymer* **2011**, *52*, 2514−2523.
(16) Shipway, A. N.; Willner, I. *Chem. Commun.* **2001**, *20*, 2035−2045.
(17) Zwijnenburg, M. A.; Illas, F.; Bromley, S. T. *J. Chem. Phys.* **2012**, *137*, 154313 (1−6)..
(18) Iijima, M.; Tsukada, M.; Kamiya, H. *J. Colloid Interface Sci.* **2007**, *307*, 418−424.
(19) Qi, C. Z.; Gao, H.; Yan, F. Y.; Liu, W. M.; Bao, G. Q.; Sun, X. D.; Chen, J. M.; Zheng, X. M. *J. Appl. Polym. Sci.* **2005**, *97*, 38−43.
(20) Srinivasan, D.; Rao, R.; Zribi, A. *J. Electron. Mater.* **2006**, *35*, 504−509.
(21) Andrade, G. I.; Barbosa-Stancioli, E. F.; Mansur, A. A. P.; Vasconcelos, W. L.; Mansur, H. S. *J. Mater. Sci.* **2008**, *43*, 450−463.
(22) Ahmed, S.; Jones, F. R. *J. Mater. Sci.* **1990**, *25*, 4933−4942.
(23) Young, S. S.; Jae, R. Y. *Carbon* **2005**, *43*, 1378−1385.
(24) Wu, C. L.; Zhang, M. Q.; Rong, M. Z.; Friedrich, K. *Compos. Sci. Technol.* **2002**, *62*, 1327−1340.
(25) Wetzel, B.; Haupert, F.; Zhang, M. Q. *Compos. Sci. Technol.* **2003**, *63*, 2055−2067.
(26) Wu, S. *Polymer* **1985**, *26*, 1855−1863.
(27) Zhang, H.; Zhang, Z.; Friedrich, K.; Eger, C. *Acta Mater.* **2006**, *54*, 1833−1842.
(28) lyu, S. P.; Zhu, X. G.; Qi, Z. N. *J. Polym. Res.* **1995**, *2*, 217−224.
(29) Norman, D. A.; Robertson, R. E. *Polymer* **2003**, *44*, 2351−2362.
(30) Sanchez-Soto, M.; Gordillo, A.; Maspoch, M. L.; Velasco, J. I.; Santana, O. O.; Martinez, A. B. *Polym. Bull.* **2002**, *47*, 587−594.
(31) Liu, Y. L.; Hsu, C. Y.; Wei, W. L.; Jeng, R. J. *Polymer* **2003**, *44*, 5159−5167.
(32) Huang, G. C.; Lee, J. K. *Composites, Part A* **2010**, *41*, 473−479.
(33) Tarrio-Saavedra, J.; Lopez-Beceiro, J.; Naya, S.; Gracia, C.; Artiaga, R. *Exp. Polym. Lett.* **2010**, *4*, 382−395.
(34) Preghenella, M.; Pegoretti, A.; Migliaresi, C. *Polymer* **2005**, *46*, 12065−12072.
(35) Sun, Y. Y.; Zhang, Z. Q.; Moon, K. S.; Wong, C. P. *J. Polym. Sci., Polym. Phys.* **2004**, *42*, 3849−3858.
(36) Kwon, S. C.; Adachi, T.; Araki, W. *Composites, Part B* **2008**, *39*, 773−781.
(37) Macan, J.; Ivankovic, H.; Ivankovic, M.; Mencer, H. J. *J. Appl. Polym. Sci.* **2004**, *92*, 498−505.
(38) Reddy, C. S.; Patra, P. K.; Das, C. K. *Macromol. Symp.* **2009**, *277*, 119−129.
(39) Isin, D.; Kayaman-Apohan, N.; Gungor, A. *Prog. Org. Coat.* **2009**, *65*, 477−483.